AGU100 ADVANCING EARTH AND SPACE SCIENCE

Geochemistry, Geophysics, Geosystems

RESEARCH ARTICLE
10.1029/2017GC007361

Key Points:
- This study, for the first time, reports the Mg isotopic composition of langbeinite, a potassium-magnesium sulfate evaporite mineral from late Permian
- Based on our study, we infer the late Permian seawater, from which langbeinite precipitated, had δ^{26}Mg <-4 ‰
- Our study demonstrates that Mg isotopic proxies can help constrain temperature conditions and relative rates of evaporation
- We describe how Mg isotopes can serve as effective tools for interpreting brine sources and diagenesis

Supporting Information:
- Supporting Information S1
- Data Set S1
- Data Set S2
- Data Set S3
- Data Set S4
- Figure S1
- Figure S2
- Figure S3
- Figure S4
- Figure S5
- Table S1

Correspondence to:
S.-C. Chang,
suchin@hku.hk

Citation:
Feng, C., Gao, C., Yin, Q.-Z., Jacobsen, B., Renne, P. R., Wang, J., & Chang, S.-C. (2018). Tracking physicochemical conditions of evaporite deposition by stable magnesium isotopes: A case study of late Permian langbeinites. *Geochemistry, Geophysics, Geosystems*, *19*, 2615–2630. https://doi.org/10.1029/2017GC007361

Received 27 NOV 2017
Accepted 18 APR 2018
Accepted article online 25 MAY 2018
Published online 18 AUG 2018

Tracking Physicochemical Conditions of Evaporite Deposition by Stable Magnesium Isotopes: A Case Study of Late Permian Langbeinites

Chongqin Feng[1], Caihong Gao[2], Qing-Zhu Yin[3], Benjamin Jacobsen[3,4], Paul R. Renne[5,6], Jun Wang[1], and Su-Chin Chang[1]

[1]Department of Earth Sciences, The University of Hong Kong, Hong Kong Special Administrative Region, Hong Kong, [2]State Key Laboratory of Ore Deposit Geochemistry, Institute of Geochemistry, Chinese Academy of Sciences, Guiyang, China, [3]Department of Earth and Planetary Sciences, University of California at Davis, Davis, CA, USA, [4]Now at Lawrence Livermore National Laboratory, Livermore, CA, USA, [5]Berkeley Geochronology Center, Berkeley, CA, USA, [6]Department of Earth and Planetary Science, University of California at Berkeley, Berkeley, CA, USA

Abstract Magnesium isotopic compositions of evaporite deposits may record information concerning brine evolution during deposition. We report Mg isotopic values ($\delta^{26}Mg_{DSM3}$) measured from an evaporite deposit of langbeinite ($K_2Mg_2(SO_4)_3$) found in the Permian Salado Formation. We used these data to model Mg isotope fractionation between langbeinite and its parent brine. In addition, both measured and theoretical results are used to estimate precipitation temperature and interpret depositional environment. The Salado langbeinite δ^{26}Mg values are relatively low and fall within a relatively narrow range (–4.12 ± 0.03‰ to −3.81 ± 0.07‰). Equilibrium fractionation factors between langbeinite and aqueous Mg^{2+} solutions were calculated using quantum chemical density functional theory. All computations were performed at the B3LYP/6-31 + G(d,p) level. Solvation effects were addressed using a solvent model ("water-droplet" approach) and mineral structures were investigated using volume variable cluster models (VVCM). The equilibrium Mg isotopic fractionation factors α between langbeinite and model brine solution we obtained are 1.0005, 1.0004, and 1.0003 ($\Delta^{26}Mg_{langb\text{-}water} \approx 10^3 \ln\alpha = 0.473‰$, 0.390‰, and 0.322‰) at 10°C, 25°C, and 40°C, respectively. These relatively large equilibrium fractionation factors indicate significant Mg isotope fractionation between langbeinite and its parent brine during precipitation, as langbeinite preferentially incorporates the heavier ^{26}Mg and ^{25}Mg isotopes. Rayleigh distillation modeling of the Salado langbeinite's relatively light Mg isotopic composition requires $\delta^{26}Mg_{DSM3}$ values of −4‰ for the parent brine. Models favor a precipitation temperature as high as 40°C under equilibrium conditions. Potential disequilibrium precipitation conditions suggested by Mg isotopic data also imply rapid deposition in a hot, arid sedimentary environment prevailing in the southwestern U.S. during the Late Permian.

Plain Language Summary This study, for the first time, reports the Mg isotopic composition of langbeinite, a potassium-magnesium sulfate evaporite mineral from late Permian. Based on our study, we infer the late Permian seawater, from which langbeinite precipitated, had $\delta^{26}Mg < -4$ ‰. Our study demonstrates that Mg isotopic proxies can help constrain temperature conditions and relative rates of evaporation. We describe how Mg isotopes can serve as effective tools for interpreting brine sources and diagenesis.

1. Introduction

Evaporite deposition depends strongly on the origin and evolution of parent brines. In the case of ancient sedimentary deposits, isotopic compositions of evaporites may offer important remnant geochemical evidence of their parent brines. Given accurate estimates of the relevant isotopic fractionation factors, these chemical parameters may provide proxy evidence of brine chemistry. Magnesium is a rock forming element, a major element in fresh water, and the second most abundant cation in seawater (Wright and Colling (1995); Millero, 1974). A better understanding of Mg isotope chemistry can thus help constrain models for brine chemistry and brine evolution. Reconstructing brine evolution using Mg isotopic data requires detailed knowledge of Mg isotopic fractionation between parent brine and evaporites.

Advances in analytical instrumentation have enabled high-precision Mg isotope measurements of various evaporites deposits and relevant sedimentary minerals. Many studies have reported that carbonates typically exhibit lighter Mg isotopic compositions than silicates (i.e., Blattler et al., 2015; Buhl et al., 2007; Fantle & Higgins, 2014; Galy et al., 2002; Higgins & Schrag 2010, 2012, 2015; Kasemann et al., 2014; Liu et al., 2014; Opfergelt et al., 2014; Pogge von Strandmann et al., 2012; Wimpenny et al. 2014; Wombacher et al., 2011). To further understand the Mg isotopic feature observed in the evaporite deposits samples, many studies made efforts to investigate the Mg isotopic fractionation between aqueous solutions and Mg evaporites and other relevant sedimentary minerals (i.e., Higgins & Schrag 2010; Immenhauser et al., 2010; Li et al. 2011, 2012, 2015; Wang et al., 2013). Because carbonates and silicates are common Mg sinks present in an evaporite and relevant sedimentary depositional sequence, most of previous research only focused on Mg-bearing carbonates and silicates (i.e., Higgins & Schrag 2010; Immenhauser et al., 2010; Li et al., 2012, 2015; Mavromatis et al., 2012, 2013; Pearce et al., 2012; Pogge von Strandmann 2008; Rustad et al. 2010; Saulnier et al., 2012; Schauble 2011; Wang et al., 2013). Using experimental calibrations, theoretical calculations, and well-characterized natural samples, many previous studies have found that Mg-carbonates tend to exhibit a large (1–4‰) and negative Mg isotopic fractionation between mineral and fluids (i.e., $\Delta^{26}Mg_{calcite-fluid} = \delta^{26}Mg$ of calcite-$\delta^{26}Mg$ of fluid $= -2.2‰$ at 45°C, Li et al., 2012; $\Delta^{26}Mg_{dolomite-water} = -3.1$ ‰ at 25°C, Schauble, 2011), although some other studies proposed different fractionation factors with different magnitudes or even the direction (i.e., Rustad et al., 2010). In contrast, Mg-silicates like clay typically have a relatively large but positive Mg isotopic fractionation between mineral and fluid (i.e., $\delta^{26}Mg_{clay}$-$\delta^{26}Mg_{pore-fluid}$ is 0 to $+1.25‰$, Higgins & Schrag 2010).

Magnesium-bearing sulfates are also a common Mg sink during evaporite formation, especially in sabkhas, salt lakes, lagoons, restricted ocean basins, and ancient surface areas of Mars. Very little information is available for Mg isotopic composition or Mg isotopic fractionation factors for natural Mg-sulfates. To our knowledge, only two studies have investigated Mg isotopic fractionation between Mg-sulfates and aqueous solutions. Li et al. (2011) reported a relatively constant Mg isotopic fractionation factor between synthetic epsomite ($MgSO_4{\blacksquare}7H_2O$) and a $MgSO_4$ solution based on a series of recrystallization experiments ($\Delta^{26}Mg_{eps-solution} = +0.56‰$ to $0.63‰$ from 7 to 40°C). Shalev et al., (2014) reported a Mg isotopic fractionation of about $-1.2‰$ between kainite ($MgSO_4{\blacksquare}KCl{\blacksquare}3H_2O$) and brine. These researchers suggested that Mg isotopic compositions of sulfates can record hydrogeochemical factors influencing the brine, such as restriction of the evaporitic basin and/or secular variation of $\delta^{26}Mg$ in seawater. However, using Mg isotopic geochemistry to constrain the hydrological evolution for the brine of Mg-sulfates still requires further combinations of both systematic isotopic data for natural samples and relevant fractionation factors for data interpretation.

This study analyzed samples from a well-studied langbeinite ($K_2Mg_2(SO_4)_3$) bearing evaporite profile in the Upper Permian Salado Formation of the Delaware Basin in southeastern New Mexico, USA. This langbeinite profile lends itself to the interpretation of Mg isotopic systematics due to the uniform prevalence of langbeinite throughout the deposit and the availability of precise radioisotopic ages for the langbeinite section (Renne et al., 2001). The absence of Mg-bearing silicate and carbonate phases also simplifies interpretation of Mg isotopic fractionation dynamics since opposite Mg fractionation directions for these phases relative to aqueous solutions might complicate interpretation of isotopic signatures (Galy et al., 2002; Higgins & Schrag 2015; Schauble 2011; Tipper et al., 2006b; Young & Galy, 2004). In addition to reporting a radioisotopic age for the deposit, Renne et al., (2001) also measured its sulfur isotopic compositions. Several reports have described the depositional environment in detail (Holser & Magaritz, 1987; Lowenstein, 1988; Renne et al., 2001), thus providing additional critical constraints on Mg isotope data interpretation.

In addition to reporting Mg isotope data from the Salado langbeinite, this research also estimated equilibrium Mg isotope fractionation factors between langbeinite and its parent brine in order to interpret the Mg isotopic chemistry of the brine. Laboratory methods cannot easily achieve equilibrium conditions necessary to measure Mg isotopic fractionation factors. Theoretical quantum chemistry calculations, however, can model equilibrium isotopic exchange scenarios. This method has been widely applied in calibrating equilibrium isotopic fractionation between minerals and solution for a range of stable isotope systems, including O, B, Ca, Fe, and Mg (e.g., Javoy et al., 2012; Kowalski et al., 2013; Méheut et al., 2007; Pinilla et al., 2015; Rustad et al., 2010; Schauble, 2011). For example, Rustad et al. (2010), Schauble (2011), and Pinilla et al. (2015) have used quantum chemistry models to estimate Mg isotopic fractionation factors between Mg-

carbonates and solution. Specifically, using cluster method, Rustad et al. (2010) embedded a cluster of $Mg(H_2O)_{18}^{2+}$ with single configuration in continuum solvent model to simulate aqueous environment, and obtained similar reduced isotope partition function ratio (RPFR) values for $^{26}Mg/^{24}Mg$ in solution with that reported by Pinilla et al. (2015). Nevertheless, by using hexaaqua-magnesium crystal to represent the aqueous phase, Schauble (2011) reported higher values than those data of Rustad et al. (2010) and Pinilla et al. (2015) (e.g., 25.5 versus 22.6–23.5 of 10^3ln RPFR at 25°C). In this study, we use water-droplet procedure (Li & Liu, 2015; Liu, 2013; He et al., 2016) to simulate the solution phase with various water molecules and consider the effect of the configuration disorder on RPFR (Pinilla et al., 2015) to obtain RPFR($^{26}Mg/^{24}Mg$) for solution. Finally we use these data to estimate Mg isotopic fractionation factor between langbeinite and solution.

When applied to interpreting the Salado langbeinite Mg isotopic compositions, our calculations help to illustrate the precipitation temperature and hydrological restriction for the langbeinite salts. Furthermore, this study constrains the brine source for the Salado langbeinite based on the Mg isotopic feature suggested by the measured Mg isotopic composition of the langbeinites and our theoretical fractionation factors.

2. Geologic Setting

The Permian Salado Formation occurs in the Delaware Basin of west Texas and southeastern New Mexico. The formation contains an evaporite sequence that reaches thicknesses of 700 m in the subsurface (Lowenstein, 1988) and is interpreted to represent a typical marine sequence formed in a shallow water and low-relief depositional environment (Stein & Krumhansl, 1988). Along with the overlying Rustler Formation and underlying Castile Formation, the Salado Formation developed during the Ochoan stage of the Late Permian. The overlying Rustler Formation mainly comprises massive thick beds of halite and anhydrite-polyhalite (Lowenstein, 1988). The Castile Formation is composed, by volume, of about 50% halite, 45% anhydrite, and 5% calcite (Anderson, 1981). The Salado formation was devided into three unites and it consists of halite, anhydrite, gypsum, clay interbedded with carbonates and potassium-enriched intervals (Abitz et al., 1990; Stein & Krumhansl, 1988). The stratigraphy and the mineralogy of the Ochoan evaporite sequences are summaried in Figure 1.

The langbeinite samples analyzed by this study occur in the McNutt zone, a horizon in the middle of the Salado Formation that is extensively mined for potash. Langbeinite samples were collected from a subsurface mine in a section spanning about 100 m within the McNutt potash zone. Our sampling site consists mostly of langbeinite. Sampling points occurred within a single sequence at specific depths of 150, 212, and 257 m (sample i.d.s: IMC-1, IMC-3, and IMC-2, respectively). Renne et al. (2001) used $^{40}Ar/^{39}Ar$ methods to obtain a radiometric age of about 251 Ma for this part of the section.

During the Late Permian, the Salado Formation probably developed along the western margin of Pangea as a marginal area of the Panthalassa Ocean near the paleo-equator (5–10° N, see Figure 2) (Kirkland et al., 2000; Golonka et al., 1994; Scotese, 1994). The Delaware basin became restricted in the late Guadalupian Stage, probably due to eustatic sea level fall (Forney, 1975). Basin restriction coupled with high rates of evaporation of equatorial areas caused a progressive increase in salinity evident from massive evaporite deposits and other indicators of hypersaline conditions.

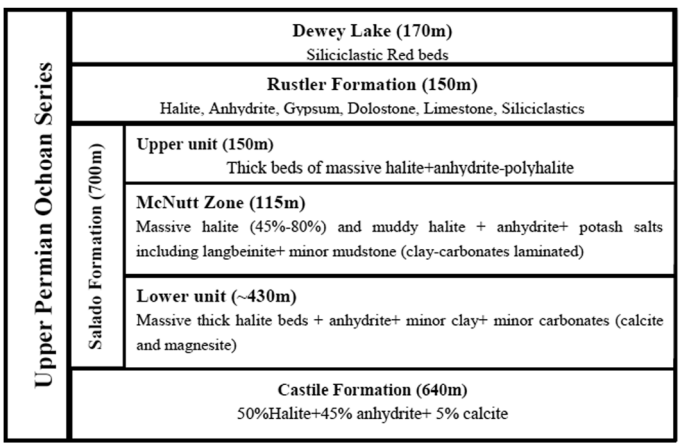

Figure 1. Stratigraphy of the Ochoan Series, Deleware Basin. The maximum thickness of each Formation is also given. The mineralogy is summaried from Anderson (1981); Abitz et al. (1990), and Stein and Krumhansl (1988).

3. Methods

Before isotopic analysis, we verified mineralogy and determined specific compositions for langbeinite samples using X-ray diffraction and scanning electron microscope (SEM) imaging analysis. This data are given in the supporting information Figures S1 and S2, Table S1.

3.1. Mg Isotope Preparation Procedures and Mass Spectrometric Analysis

All chemical separation procedures and analyses were conducted at the University of California, Davis (UC Davis), following methods described in Black et al. (2008) and Jacobsen et al. (2008).

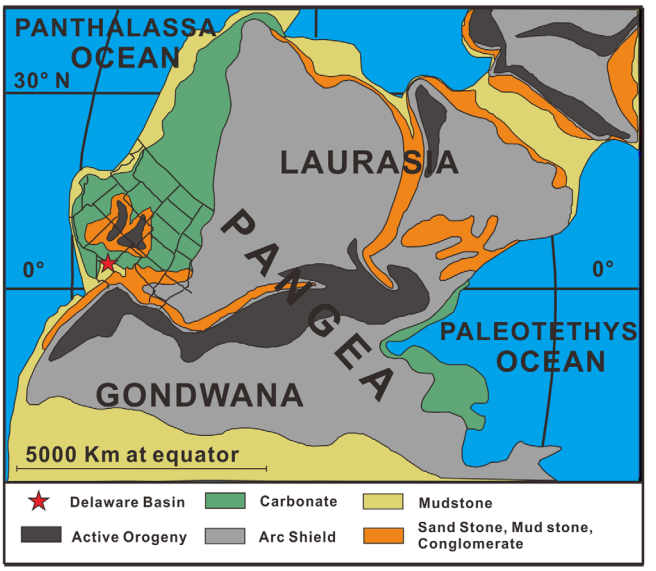

Figure 2. Paleogeography of the Late Permian Delaware Basin located along the western margin of Pangea and bordering the Panthalassa Ocean at ~5–10°N latitude. The location likely represents a warm, arid environment that experienced high evaporation rates, possibly similar to modern conditions in equatorial east Africa (Kutzbach & Gallimore, 1989; Parrish et al., 1986). Map representation is revised after Blakey (2004) http://jan.ucc.nau.edu/~rcb7/270NAt.jpg. Langbeinite samples were collected from the Salado Formation, Delaware Basin, southeastern New Mexico, USA (red star).

Briefly, sample powders were digested with 3 mL of concentrated HF-HNO_3 (3:1 volume ratio) in Teflon beakers. The residues were dissolved in 1 mL of concentrated HNO_3 to remove residual fluorides and then conditioned with 1 mL 2*N* HNO_3 for ion-exchange chromatography. A column filled with 2 mL AG50W-X12 (200–400 mesh) cation resins were rinsed following methods described in Chang et al. (2003) prior to loading samples for ion exchange chromatography. After being loaded, the analyte was eluted with 3 mL 1*N* HNO_3. Additional aliquots of 1*N* HCl, 1*N* HNO_3 + 0.5*N* HF, and 2*N* HNO_3 were used to elute Cr, Al, Fe, Na, and K before collecting Mg. Mg^{2+} eluted after passing approximately 20–35 mL of a 2*N* HNO_3 acid solution through the columns. This chromatographic procedure provided adequate Mg yields of ~99.5% (Black et al., 2008) and the blank was ~0.3% relative to the total Mg in the samples. Solutions of separated pure Mg were evaporated and then diluted in 25 mL 0.1*N* HCl to obtain sample solutions with Mg concentrations in the approximate range of ~400 ppb.

Mg isotope ratios were measured with a Nu Plasma multicollector inductively coupled plasma mass spectrometer (MC-ICP-MS) at UC Davis. A DSN-100 desolvating nebulizer aspirated samples to the plasma source using a dilute 1*N* HCl solution. The measurements were made in the static and pseudo-high-resolution mode. Each analysis included four baseline measurements of 60 s duration and 180 s of Mg signal acquisition. The standard-sample bracketing technique was used to calibrate signal drift and instrument fractionation. The standard DSM3 (Galy et al., 2003) was used as the bracketing standard. Mg isotopic values are presented in standard delta notation using the equation $\delta^{x}\mathrm{Mg} = [(^{x}\mathrm{Mg}/^{24}\mathrm{Mg})_{\mathrm{sample}}/(^{x}\mathrm{Mg}/^{24}\mathrm{Mg})_{\mathrm{DSM3}}\text{-}1]\times 1{,}000$, where x = 26 or 25. Precision for the Cambridge-1 standard during analysis was ±0.128‰ for δ^{26}Mg and ±0.061‰ for δ^{25}Mg (2σ).

3.2. Theoretical Basis

3.2.1. Fractionation Factor Calculation Theory

Fractionation factor calculations assumed the basic isotope exchange reaction

$$\mathrm{AX} + \mathrm{BX}* \leftrightarrow \mathrm{AX}^{*} + \mathrm{BX} \tag{1}$$

In this system, phases A and B contain element X, and X* represents the heavier isotope within the AX + BX system. The equilibrium isotope exchange constant (K) can be represented as the ratio of the reduced isotope partition function ratio (RPFR) for the two phases:

$$K = RPFR\ (AX*/AX)/RPFR\ (BX*/BX). \tag{2}$$

The RPFR (also named β) for each phase is given by the following equation:

$$\mathrm{RPFR}(AX^{*}/AX) = \frac{s^{*}}{s} f = \prod_{i}^{3n-6} \frac{u_i(AX^{*})\exp\left[-u_i(AX^{*})/2\right]\{1-\exp\left[-u_i(AX)\right]\}}{u_i(AX)\exp\left[-u_i(AX)/2\right]\{1-\exp\left[-u_i(AX^{*})\right]\}} \tag{3}$$

where *s* is the molecule's symmetry number, *i* is a running index of vibrational modes, and *n* is the atom number and the product on the right-hand of the equal sign in (3) covering all 3n-6 phonon modes. Critically, u_i is defined as

$$u_i = \mathrm{h}\omega_{\mathrm{i}}/\mathrm{kT} \tag{4}$$

where h is Plank's constant, k is the Boltzmann constant, T is temperature in kelvins and ω_{i} is the vibrational frequency of the i-th mode.

The fractionation factor α ($\alpha_{\mathrm{A-B}} = \frac{\mathrm{R_A}}{\mathrm{R_B}} = \frac{(\mathrm{X}^{*}/X)_A}{(\mathrm{X}*/X)_B}$) is a function of the exchange constant, a relation generally given as $\alpha = \mathrm{K}^{1/\mathrm{n}}$, where n is the number of atoms exchanged in the reaction equation (1). In our study,

n = 1 for Mg isotope exchange, rendering $\alpha = K$. Since this study calibrates the Mg isotopic fractionation factor between langbeinite and brine solution, the equation could be given specifically as

$$\alpha_{langb-water} = \frac{\left({}^{26}Mg/{}^{24}Mg\right)_{langb}}{\left({}^{26}Mg/{}^{24}Mg\right)_{water}} = \frac{RPFR\left({}^{26/24}Mg_{langb}\right)}{RPFR\left({}^{26/24}Mg_{water}\right)}. \quad (5)$$

As shown in equations (3)–(5), determination of the fractionation factor depends on obtaining RPFRs for the relevant molecules, an operation which requires accurately estimated vibrational frequencies (ω) (Bigeleisen & Mayer, 1947; Urey, 1947).

3.2.2. Fractionation Factor Calculation

In this study, we used the volume variable cluster model (He et al., 2016; Li & Liu, 2015; Liu, 2013) to calculate RPFRs for $^{26}Mg/^{24}Mg$ in langbeinite. The *American Mineralogist Crystal Structure Database* provided langbeinite lattice parameters (http://rruff.geo.arizona.edu/AMS/amcsd.php) for simulating crystal structure. The initial langbeinite crystal used in modeling was based on the langbeinite structure reported in Mereiter (1979). Cluster size was set so as to optimize the reliability of the results according to computational limitations. Because there are two different Mg sites in the langbeinite lattice (M_1 and M_2), we built two langbeinite cluster models in which Mg atoms occupy respective M_1 and M_2 sites (supporting information Figures S3a and S3b). In order to use computational resources efficiently, we only computed vibrational frequencies for the Mg atoms and for six SO_4^{2-} ions occupying the inner layer and surrounded by other atoms fixed in their optimized positions. For the sake of simplicity, we ignored the effects of K^+ in the hypothetical solution. While we cannot rule out interference or incorporation of other ions, these should represent only minor effects. Point charges were introduced at the edges of the langbeinite cluster structure to neutralize its total valence. We searched for an optimal configuration with the lowest total energy by varying the distance of the electric charge. After specifying and optimizing an appropriate langbeinite structure, the relevant vibrational frequencies were derived from a force constant matrix.

We considered the range of Mg species documented in brine/fluid systems (Akilan et al., 2006; Buchner et al., 2004; Jahn & Schmidt, 2010) and chose species that best characterized brines providing stable conditions for langbeinite formation. These species include (1) single Mg^{2+} cation, (2) double solvent separated ion pairs (2SIP,$Mg(H_2O)_2SO_4$), (3) contact ion pairs (CIP,$MgSO_4$), and (4) single solvent separated ion pairs (SIP,$Mg(H_2O)SO_4$). Because the SO_4^{2-} species exert only minor influence on the Mg cation in 2SIPs, we treated the 2SIP model as a single Mg^{2+} cation model, which also helped simplify the simulation. The model, therefore, used species (1), (3), and (4) to simulate brine evolution (see supporting information Figures S4a, S4b, and S4c).

To simulate solvation effects in the aqueous environment, we used the multistep "water droplet" procedure (see Liu & Tossell, 2005 for details). This method assumes a set of 6–36 water molecules surrounding a Mg^{2+} ion in solution to simulate solvation effects. Liu and Tossell (2005) used this method for predicting boron isotope fractionation between $B(OH)_3$ and $B(OH)_4$ in seawater. Similar method was proven effective in calculating fractionation factors between solid and aqueous phase pairs (Rustad & Bylaska, 2007; Rustad et al., 2010). We also used $Mg(H_2O)_6^{2+}$ to represent the first solvation shell given that Mg^{2+} is mostly hexacoordinated in the aqueous phase, as shown by both experimental and computational studies (Markham et al., 2002; Ohtaki & Radnai, 1993). The initial hydration configuration surrounded each Mg atom with six H_2O molecules (i.e., the water droplet). The procedure then optimized the configuration and calculated frequencies. The procedure was repeated after adding another six H_2O molecules. As the number of water molecues larger than 24, we found that optimization barely modified the configuration of the inner H_2O molecules. We included up to 36 H_2O molecules in the set of hydration configurations analyzed. This number of H_2O molecules should provide reliable results since previous studies accurately modeled Ge and V isotopic behavior using 30 and 24 H_2O molecules, respectively (Li et al., 2009; Li & Liu, 2010; Wu et al., 2015). We used four different optimized configurations for each step, calculated vibrational frequency and then averaged values among the four configurations.

All calculations were performed using the Tianhe Unit 2 computer cluster at the Guangzhou supercomputer center. The langbeinite and aqueous phases were both simulated using the Gaussian09 software package (Frisch et al., 2009) and assuming the same B3LYP/6–31 + G(d,p) level. We also checked vibrational frequencies of Mg for $Mg(H_2O)_6^{2+}$ at higher B3LYP/6–311++G(2df,2pd) and B3LYP/aug-cc-pVTZ levels as well. These tests showed that the vibrational frequencies calculated for levels higher than B3LYP/6–31 + G(d, p)

Table 1
Vibrational Frequencies for Mg of $Mg(H_2O)_6^{2+}$ as Calculated in This Study or Reported in Literature Sources

	Vibrational frequencies (cm^{-1})	
	Antisym-streching	Sym-strecthing
B3LYP/6–311++G(d,p)[a]	249	314
B3LYP/aug-cc-pVTZ[a]	246	318
Exp[a,b]	314	355
B3LYP/6–311++G(2df,2pd)[c]	249	318
B3LYP/aug-cc-pVTZ[c]	249	318
B3LYP/6–311++G(2d,2p)[c]	250	316
B3LYP/6–31+G(d,p)[c]	251	315

[a]Data from Kapitán et al. (2010). [b]Infrared spectroscopy data from Mink et al. (2003). [c]Data calculated by this study.

differed only by about 0.8‰ at 25°C (Table 1). This sensitivity test demonstrated that the assumed theoretical level provided accurate results adequate for the purposes of this study.

4. Results

4.1. Equilibrium Isotope Fractionation Between Langbeinite and Aqueous Mg

4.1.1. Comparison of Vibrational Frequencies

Uncertainties in our calculations may arise from frequency errors related to the influence of vibrational frequency on RPFR value (see section 3.2.1). Among the vibrational frequency components, we identified three of the degenerated bending modes for the langbeinite configuration in which Mg atoms occupy the M_1 site (360, 363, and 368 cm^{-1}) and three for the configuration in which Mg atoms occupy the M_2 site (340, 353, and 357 cm^{-1}) (supporting information Table S2).

For the aqueous models, we compared vibrational frequencies estimated for $Mg(H_2O)_6^{2+}$ with other published data reported at the B3LYP/6–31++G(d,p), and B3LYP/aug-cc-pVTZ levels (see Table 1). Our results agree well, even for different basis sets, with those reported from ab initio calculations in Kapitán et al. (2010).

4.1.2. Model Crystal Structures and RPFRs

Supporting information Figures S3 and S4 show models of the optimized langbeinite crystal and aqueous Mg species configurations. The Mg cations in both langbeinite sites ($K_2Mg_2(SO_4)_3$) are hexacoordinated. The mean Mg-O bond lengths for optimized langbeinite structures in which Mg atoms occupy M_1 and M_2 sites are 2.047 Å and 2.070 Å, respectively. These values are consistent with the 2.048-2.050 Å range for M_1-O and the 2.053-2.075 Å range for M_2-O reported in Speer and Salje (1986) (see supporting information Table S3). Supporting information Table S3 lists mean Mg-O bond distances of all four optimized configurations for a series of hydration configurations containing 6, 12, 18, 24, 30 and 36 water molecules. Supporting information Table S3 also provides theoretical and experimental data on $Mg(H_2O)_6^{2+}$ from additional literature sources for comparison. To characterize the solution phase, which included single Mg^{2+} ions and other complexed species, we chose a mean Mg-O bond distance for the aqueous Mg species ranging from 2.105 to 2.119 Å. This range exceeded the 2.047 (M_1) Å and 2.070 (M_2) Å bond lengths for the langbeinite crystal lattice estimated by our calculations. The calculated bond distance for $Mg(H_2O)_6^{2+}$ agreed well with theoretical results reported in literature sources but exceeded empirically determined values (2.102 versus 2.063 and 2.067 Å). The causes for these differences remain uncertain. In addition to assumptions of low pressure conditions, other uncertainties or sources of calculation error may contribute to this discrepancy.

Table 2 gives RPFR values for $^{26}Mg/^{24}Mg$ as aqueous Mg species and various hydration configurations calculated at 25°C. The four configurations for each aqueous species give slightly different RPFRs even for models containing the same number of water molecules, thus demonstrating the importance of conformational sampling. As described in section 3.2.2, our simulation of Mg in the aqueous environment assumes a series of hydration configurations to calculate RPFR. We find that the RPFR varies as the number of water molecules increases, but stabilizes once a critical number of water molecules surround the Mg cation. Supporting information Figure S5 shows that once the number of water molecules exceeds 24, the average RPFRs converge upon a constant value that ranges from 1.02676 to 1.02685. These results demonstrate the effectiveness and stability of our simulation methods. To obtain reliable RPFR estimates, we calculated the average RPFR of all configurations for species hydrated by 24, 30, and 36 water molecules. Our approach gave a standard deviation (σ) of 0.5‰ for the average RPFR.

At a certain temperature, differences in bond length, coordination number, oxidation state, and spin state can influence equilibrium isotope fractionation between two phases. Generally, shorter bond lengths or lower coordination states result in heavy isotope enrichment (and vice versa). Isotopes of Fe, Ca, and Mg show similar effects in various systems including magma-mineral pairs (e.g., Feng et al., 2014; Huang et al., 2013; Young et al., 2015). As shown in Table 2 and supporting information Table S3, aqueous Mg species

Table 2
RPFRs for $^{26}Mg/^{24}Mg$ in Different Aqueous Mg Hydration Configurations at 25°C

Cluster	RPFR[a]	Cluster	RPFR[a]	Cluster	RPFR[a]
$Mg(H_2O)_{24}^{2+}$_A	1.02563	$Mg\text{-}SO_4(H_2O)_{24}^{2+}$_A	1.02654	$Mg\text{-}H_2O\text{-}SO_4(H_2O)_{23}^{2+}$_A	1.02645
$Mg(H_2O)_{24}^{2+}$_B	1.02589	$Mg\text{-}SO_4(H_2O)_{24}^{2+}$_B	1.02540	$Mg\text{-}H_2O\text{-}SO_4(H_2O)_{23}^{2+}$_B	1.02527
$Mg(H_2O)_{24}^{2+}$_C	1.02640	$Mg\text{-}SO_4(H_2O)_{24}^{2+}$_C	1.02540	$Mg\text{-}H_2O\text{-}SO_4(H_2O)_{23}^{2+}$_C	1.02570
$Mg(H_2O)_{24}^{2+}$_D	1.02569	$Mg\text{-}SO_4(H_2O)_{24}^{2+}$_D	1.02670	$Mg\text{-}H_2O\text{-}SO_4(H_2O)_{23}^{2+}$_D	1.02495
Average	**1.02590**	Average	**1.02601**	Average	**1.02559**
$Mg(H_2O)_{30}^{2+}$_A	1.02689	$Mg\text{-}SO_4(H_2O)_{30}^{2+}$_A	1.02692	$Mg\text{-}H_2O\text{-}SO_4(H_2O)_{29}^{2+}$_A	1.02590
$Mg(H_2O)_{30}^{2+}$_B	1.02666	$Mg\text{-}SO_4(H_2O)_{30}^{2+}$_B	1.02561	$Mg\text{-}H_2O\text{-}SO_4(H_2O)_{29}^{2+}$_B	1.02537
$Mg(H_2O)_{30}^{2+}$_C	1.02639	$Mg\text{-}SO_4(H_2O)_{30}^{2+}$_C	1.02574	$Mg\text{-}H_2O\text{-}SO_4(H_2O)_{29}^{2+}$_C	1.02600
$Mg(H_2O)_{30}^{2+}$_D	1.02600	$Mg\text{-}SO_4(H_2O)_{30}^{2+}$_D	1.02571	$Mg\text{-}H_2O\text{-}SO_4(H_2O)_{29}^{2+}$_D	1.02456
Average	**1.02649**	Average	**1.02600**	Average	**1.02545**
$Mg(H_2O)_{36}^{2+}$_A	1.02665	$Mg\text{-}SO_4(H_2O)_{36}^{2+}$_A	1.02566	$Mg\text{-}H_2O\text{-}SO_4(H_2O)_{35}^{2+}$_A	1.02622
$Mg(H_2O)_{36}^{2+}$_B	1.02679	$Mg\text{-}SO_4(H_2O)_{36}^{2+}$_B	1.02553	$Mg\text{-}H_2O\text{-}SO_4(H_2O)_{35}^{2+}$_B	1.02545
$Mg(H_2O)_{36}^{2+}$_C	1.02600	$Mg\text{-}SO_4(H_2O)_{36}^{2+}$_C	1.02608	$Mg\text{-}H_2O\text{-}SO_4(H_2O)_{35}^{2+}$_C	1.02589
$Mg(H_2O)_{36}^{2+}$_D	1.02611	$Mg\text{-}SO_4(H_2O)_{36}^{2+}$_D	1.02643	$Mg\text{-}H_2O\text{-}SO_4(H_2O)_{35}^{2+}$_D	1.02497
Average	**1.02639**	Average	**1.02592**	Average	**1.02563**
Preferred value[b]					**1.02599**
Langbeinite (M_1)					1.02741
Langbeinite (M_2)					1.02537
Average					**1.02639**
$\alpha_{langb\text{-}aq}$					**1.00039**

[a]RPFR uncalibrated. [b]Preferred value is the mean value of single aqueous Mg cation ($Mg(H_2O)_{24}$, $Mg(H_2O)_{30}$, $Mg(H_2O)_{36}$), CIP ($Mg\text{-}SO_4(H_2O)_{30}$ and $Mg\text{-}SO_4(H_2O)_{36}$), and SIP $Mg\text{-}H_2O\text{-}SO_4(H_2O)_{29}$ and $Mg\text{-}H_2O\text{-}SO_4(H_2O)_{35}$).

gave smaller RPFR values and longer Mg-O bond lengths than those calculated for langbeinite. This means that langbeinite precipitation favors heavier Mg isotopes while the lighter isotopes (i.e., ^{24}Mg) preferentially remain in solution.

4.1.3. Equilibrium Mg Isotope Fractionation Factors

RPFRs of Mg isotopes for the various species of aqueous Mg species analyzed in this study (aqueous Mg^{2+}, CIP, and SIP) are plotted in Figure 3 (also see supporting information Data sets S1). Figure 4 shows average isotopic RPFR values for solution and langbeinite in this study, and also lists isotopic RPFR values of Mg solutions reported in different literature sources for comparison (also see supporting information Data sets S2).

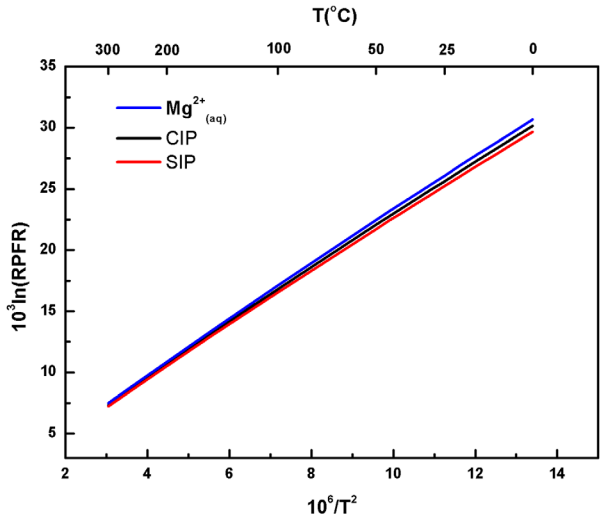

Figure 3. Mg isotope RPFRs for aqueous Mg species considered by this study (single Mg^{2+}, CIP, and SIP). The T term on the *x*-axis is in degrees Kelvin.

Figure 3 illustrates how different aqueous Mg species generate different Mg isotopic compositions. The relative magnitudes of RPFR values ($Mg^{2+}_{(aq)} > CIP > SIP$) indicate that the aqueous Mg^{2+} would assume the heaviest Mg isotopic composition, followed by the CIP and SIP species. The Mg isotopic composition of the brine depends on the proportion of these species in the brine system. In our study, we assume equal ratios for each species and thus use the average Mg isotopic RPFR for these species to represent the Mg isotopic RPFR of the brine. Figure 4 shows that the average Mg isotopic RPFR of aqueous Mg in our study is consistent with that reported in Schauble (2011) which are the average value of various hexaaqua-Mg species. Rustad et al. (2010) and Pinilla et al. (2015) reported similar RPFR of aqueous Mg^{2+} but lower than our average value (see supporting information Table S4).

Supporting information Table S5 lists Mg isotope fractionations between langbeinite and model solution ($\Delta^{26}Mg_{langb\text{-}water}$) at different temperatures along with the fitted temperature function. The $\Delta^{26}Mg_{langb\text{-}water}$ values of ~0.3–0.5‰ at 5–40°C suggest significant equilibrium Mg isotope fractionation would occur during langbeinite precipitation from its parent brine. The relatively large fractionation implies that Mg isotopic compositions of langbeinite have the potential to create significant signals for geochemical processes occurring in evaporitic environments.

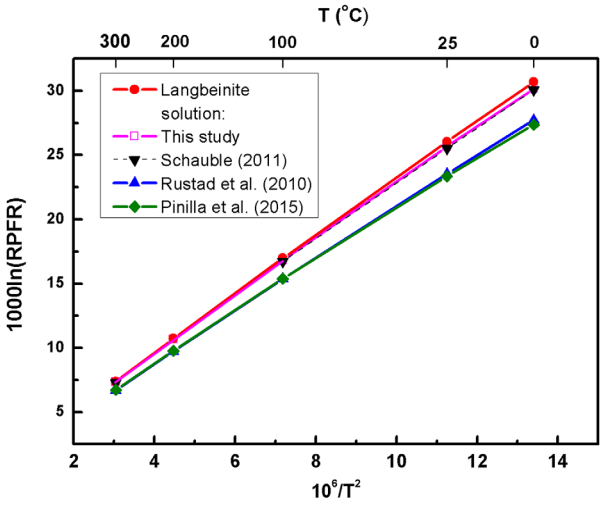

Figure 4. Mg isotope RPFRs for solution calculated by this study and values reported by previous studies at different temperatures. Here, we also plot our calculation results of RPFR for langbeinite which are higher than that of the aqueous Mg. For the RPFR of solution, our result is an average value of aqueous Mg^{2+}, CIP, and SIP. It shows good agreement with data from Schauble (2011) which is the average value of various hexaaqua-Mg species. RPFR of aqueous Mg^{2+} reported by Pinilla et al. (2015) and Rustad et al. (2010) are also given.

4.2. Mg Isotope Systematics in Langbeinites of the Upper Permian Salado Formation

Table 3 lists Mg isotopic compositions of langbeinite and standard samples relative to DSM3. Analyses of the Cambridge-1 standard and a pure Mg solution standard (Aristar Mg) agree well with results reported by other studies (see Table 3; Baker et al., 2012; Galy et al., 2003). As shown in Figure 5 and supporting information Data sets S3, langbeinite samples from this study exhibit significantly lighter Mg isotopic compositions than those from river and groundwater samples. Comparisons with data available for sulfates such as epsomite ($MgSO_4{\cdot}7H_2O$) and kainite ($MgSO_4{\cdot}KCl{\cdot}3H_2O$) further highlight the Salado langbeinite's distinctive δ^{26}Mg depletion (supporting information Data sets S3). Carbonates also have comparatively low δ^{26}Mg values relative to modern seawater. δ^{26}Mg values of some limestone samples approach those obtained here for langbeinite. Unlike limestone, dolomite, and clay values however, the langbeinite samples analyzed here spanned a stratigraphic range of 100 m and give δ^{26}Mg values within a relatively narrow range (–4.125 ± 0.060‰ to −3.814 ± 0.143‰). Excluding sample IMC2A, samples IMC2B (257 m), IMC3 (212 m), and IMC1 (150 m) give respective δ^{26}Mg values of −3.814 ± 0.143‰, −3.817 ± 0.029‰, and −3.900 ± 0.192‰.

5. Discussion

5.1. Constraining Parent Brine Characteristics From Equilibrium Mg Fractionation Factors

Our theoretical equilibrium fractionation estimates predict that langbeinite will be enriched in the heavier ^{25}Mg and ^{26}Mg isotopes relative to its parent brine. As a result, the remaining brine would have a lighter Mg isotopic composition and confer a lighter Mg isotopic composition on subsequently precipitated langbeinite. For a restricted hydrologic system, δ^{26}Mg values of langbeinite are expected to decrease with stratigraphic age as the residual brine becomes more and more enriched in ^{24}Mg. The relatively large equilibrium isotopic fractionation between langbeinite and the parent solution should further contribute to this decrease in δ^{26}Mg of langbeinite. We constructed a Rayleigh fractionation model using our calculated equilibrium Mg fractionation factor to simulate evolving Mg isotopic compositions during langbeinite precipitation (see Figure 6 and supporting information Data sets 4).

According to the standard Rayleigh distillation equation for fractional precipitation:

Table 3
Mg Isotopic Composition of Langbeinite and Standard Samples Relative to DSM3

	δ^{26}Mg (‰) ± 2σ	δ^{25}Mg (‰) ± 2σ	N	Age (Ma)[c]	Level (m)[d]
Sample					
Cambridge 1	−2.629 ± 0.128	−1.351 ± 0.061	10		
Cambridge 1[a]	−2.60 ± 0.14	−1.34 ± 0.07	35		
Aristar Mg	−1.654 ± 0.118	−0.847 ± 0.084	2		
Aristar Mg[b]	−1.584 ± 0.058	−0.819 ± 0.029	7		
Langbeinite samples					
IMC-1	−3.900 ± 0.192	−2.022 ± 0.117	4	253.3 ± 0.4	150
IMC-3	−3.817 ± 0.029	−1.982 ± 0.027	3	253.5 ± 0.6	212
IMC-2B	−3.814 ± 0.143	−1.985 ± 0.072	4	253.3 ± 0.4	257
IMC-2A	−4.125 ± 0.060	−2.143 ± 0.026	3	253.3 ± 0.4	257

Note. Upper Permian langbeinite samples spanning ~100 m stratigraphic thickness give relatively consistent Mg isotopic compositions. N indicates number of analyses. The results of standards listed above agree with results from literature sources.
[a]Data from Galy et al. (2003). [b]Data from Baker et al. (2012). [c]^{40}Ar/^{39}Ar age data recalculated from Renne et al. (2011). [d]Vertical sample positions in section.

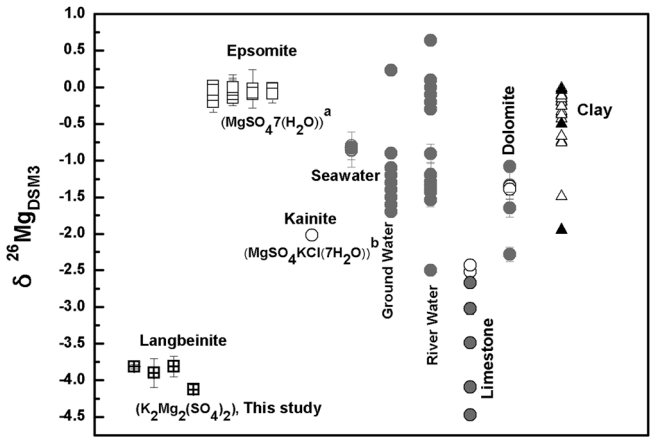

Figure 5. Measured ^{26}Mg values (relative to DSM3 standard) for sulfates, carbonates, and water samples. (a) Epsomite ($MgSO_4{\blacksquare}7H_2O$) data are from synthetic samples precipitated at equilibrium (Li et al., 2011); (b) kainite ($MgSO_4{\blacksquare}KCl{\blacksquare}3H_2O$) reported in Shalev et al. (2014); modern seawater data from Galy et al. (2002) and Tipper et al. (2006b); groundwater data from Galy et al., (2002), Ma et al. (2015), Pogge von Strandmann et al. (2008), and Tipper et al. (2006b, 2012b); river water data from Dessert et al. (2015), Galy et al. (2002), Jacobson et al. (2010), Lee et al. (2014), Pogge von Strandmann et al. (2008), and Tipper et al. (2006b, 2008, 2012a); limestone and dolomite data from Galy et al. (2002) and Tipper et al. (2006b); clay minerals data from Wimpenny et al. (2014) and Hu et al. (2017). All data in this plot could be found in supporting information Date sets S3.

$$R_w^i = R_w^0 f^{(\alpha_{j,w}-1)} \quad (6)$$

where f is the fraction of phase j (e.g., Mg in langbeinite) remaining in the aqueous solution and $f = 1\text{-}F$, where F is the fraction of Mg that is removed from solution due to the precipitation. R_w^i is ^{26}Mg/^{24}Mg remaining in solution and R_w^0 is the initial ^{26}Mg/^{24}Mg in solution. Here, $\alpha_{j,w} = {}^{26/24}\alpha_{\text{langb-water}}$. Since $\frac{R_w^i}{R_w^0} = \frac{\delta_w+1000}{\delta_0+1000}$, we can transform equation (6) to

$$\delta_w = (\delta_0+1000)\cdot f^{(\alpha_{langb-water}-1)} - 1000, \quad (7)$$

where δ_w is δ^{26}Mg of the remained solution and δ_0 is the initial δ^{26}Mg of the solution. If we further substitute equation (7) into the equation $\alpha_{langb-water} = \frac{R_{langb}}{R_{water}} = \frac{\delta_{langb}+1000}{\delta_{water}+1000}$, we could get the equation

$$\delta_{langb} = (\delta_0+1000)\cdot \alpha_{langb-water}\cdot f^{\alpha_{langb-water}-1} - 1000, \quad (8)$$

where δ_{langb} is δ^{26}Mg of langbeinite in Figure 6.

In our Rayleigh model, we set the initial Mg isotopic compositions for the parent brine varying from -4 to $-3‰$ and set a variety of temperatures to simulate the langbeinite precipitation. Simulations showed that a relatively light Mg isotopic composition (e.g., $-4‰$) was required for the parent brine to generate the observed Mg isotopic compositions of langbeinite from the Salado samples. In addition, as shown in Figure 6, langbeinite precipitation prefers high temperature. The favored temperature is as high as 40°C. This interpretation is consistent with the theoretical minimum temperature (~37°C) required for precipitation of langbeinite from a K-Na-Mg-Ca-SO_4-Cl solution (Braitsch, 1964, 1971).

Furthermore, Figure 6 suggests that overall langbeinite δ^{26}Mg values would decrease with more Mg precipitation at all temperatures due to $\alpha_{\text{langb-aq}} > 1$. We therefore conclude that δ^{26}Mg compositions in natural langbeinite evaporite sequences generally record lighter δ^{26}Mg compositions over time although some small fluctuations of temperature may be present. These systematics would especially apply to langbeinite deposited in a relatively confined system like a lagoon or restricted marine basin.

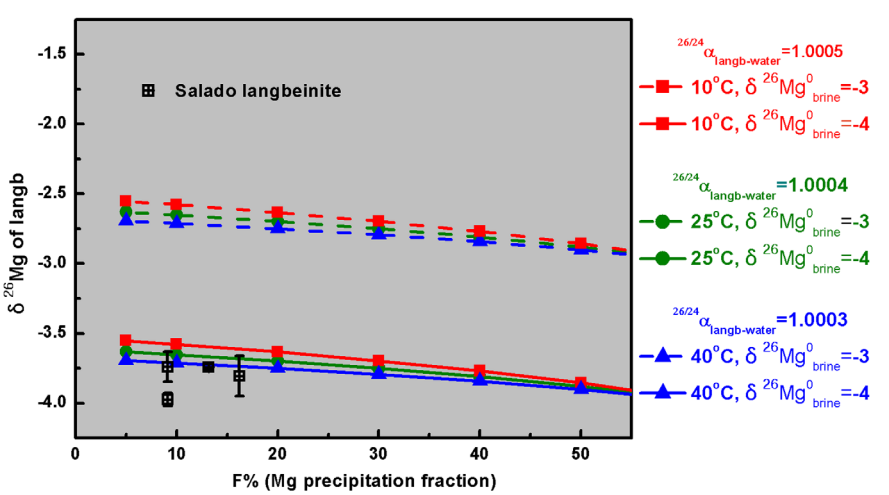

Figure 6. Rayleigh fractionation model results showing evolution of Mg isotopic compositions during langbeinite precipitation. As part of an evaporite sequence, langbeinite should exhibit monotonically decreasing δ^{26}Mg values during its progressive formation at constant temperatures. The assumed initial Mg isotopic compositions for the parent brine used in the simulations varies from -4 to $-3‰$. The natural langbeinite samples analyzed here, which span a broad stratigraphic range, show relatively uniform Mg isotopic compositions. Percent of Mg precipitated (F%) for the four langbeinite samples was estimated from thickness intervals, which may overstate F% but help contextualize the degree of isotopic uniformity.

In contrast to the closed system, sedimentary environments which receive regular seawater or freshwater input could generate different Mg isotopic signatures in langbeinite. Seawater or freshwater influx replenishes Mg incorporated in evaporites and thereby resets the Mg isotopic composition of the brine. Under these circumstances (and in contrast to the situation shown in Figure 6), δ^{26}Mg values for the langbeinite at equilibrium will not show continuous decrease but instead, occasional interruptions governed by (1) the δ^{26}Mg signature of the supplemental fluid, (2) the volume of supplemental fluid, and (3) the duration of the influx. For example, a massive and continuous influx of a fluid with a δ^{26}Mg composition similar to that of the initial brine would create relatively consistent Mg isotopic compositions in the evaporite sequence. Also, if transgression follows an evaporative cycle, langbeinite forming after the influx would have a heavier initial Mg isotopic composition than that of the langbeinite formed at the end of the last cycle, assuming that the isotopic composition of influx is similar to that of the primitive brine.

In summary, the Mg isotopic composition of langbeinite allows us to interpret the geochemical evolution of the brine from which it formed. Monotonically decreasing δ^{26}Mg values indicate langbeinite deposition in a geochemically restricted environment. Alternatively, more punctuated variation in δ^{26}Mg profiles for langbeinite deposits would theoretically indicate a more dynamic system with periodic fluid input.

5.2. Interpreting Mg Isotope Systematics From the Salado Langbeinite

The observed Mg isotopic systematics of the Salao langbeinite display especially light and uniformity features. In this section, we further discuss and analyze topics (1) the relatively light Mg isotopic compositions observed for langbeinite samples analyzed here and (2) the uniformity of δ^{26}Mg values, which does not match the expected decrease in δ^{26}Mg values with time and stratigraphic height in a restricted basin setting.

For issue (1), model calculations (see section 5.1) show that a relatively light initial parent brine can generate an isotopically light langbeinite assuming isotopic exchange reactions operating at equilibrium. If this is the case, as discussed in section 5.1, the light Mg isotopic composition of the Salado langbeinite should requires an initial parent brine with δ^{26}Mg values around to $-4‰$. Units underlying the Salado langbeinite, however, include halite, anhydrite, and carbonate deposits, as well as clay minerals (see Figure 1). The Mg isotope fractionation trends for Salado halite/anhydrite (and their parent brines) are unknown, but carbonate precipitation would generate heavier (higher) δ^{26}Mg values in brines under equilibrium conditions according to $\alpha_{\text{calcite-solution}}<1$ (e.g., Li et al., 2012; Schauble, 2011). Assuming the composition of Permian seawater contributing to the Salado Formation resembled that of modern seawater, the evaporite assemblage underlying the langbeinite analyzed here does not support inferences of a relatively light initial parent brine (e.g., δ^{26}Mg of $-4‰$). In summary, if the Salado langbeinite was formed under equilibrium conditions, the parent brine of these evaporites does not appear to be a fluid that evolved directly from seawater.

In addition to the equilibrium precipitation, kinetic isotope exchange effects also could be an alternative explanation. Isotope exchange theory asserts that the Mg isotopic exchange reaction during conversion from aqueous to solid phase must overcome an energy barrier higher than that of the reverse reaction. DePaolo (2011) estimated these energy thresholds for Ca isotopes during calcite precipitation. He found that crystal surfaces preferentially absorb the lighter Mg isotope (i.e., ^{24}Mg) due to the heightened diffusion rates and the isotope's enhanced ability to overcome the energy barrier. If this kinetic process occurs during langbeinite precipitation, langbeinite would absorb light Mg isotopes and potentially assume δ^{26}Mg values as low as those measured from the Salado samples.

For issue (2), we plot the measured δ^{26}Mg data with the simulated δ^{26}Mg systematics in Figure 6. To compare langbeinite δ^{26}Mg values, Figure 6 estimates the degree of Mg precipitation from the stratigraphic interval spanned by the samples ($\sim$50 m). The amount of Mg deposited over this thickness may actually be quite insignificant relative to the basin's seawater volume. The proportion of Mg precipitated (F%) within the stratigraphic interval sampled may thus be similarly insignificant. Given a small F% represented by the four Salado samples, the Rayleigh fractionation models can yield a similarly narrow range of δ^{26}Mg values for langbeinite. In other words, equilibrium fractionation between Salado langbeinites and their brine could account for the uniform Mg isotopic compositions.

If the Salado langbeinite Mg isotopic values reflect equilibrium fractionation processes, the measured Mg isotopic values would accordingly require relatively high depositional temperatures to achieve the equilibria

for isotopic exchange (i.e., higher temperatures facilitate isotope exchange). According to $^{40}Ar/^{39}Ar$ geochronologic results, the four langbeinite samples formed within a relatively brief (less than ~1 Ma) time interval (Renne et al., 2001). Given these constraints, the observed Mg isotopic compositions would require relatively high temperatures in the depositional environment to achieve an isotopic equilibrium within such a short depositional time frame.

In addition to the precipitation ocurred in a restrict system, as previously discussed in section 5.1, an influx of seawater could also be a candidate reason for the relatively uniform Mg isotopic composition observed in the langbeinites analyzed here. Li et al. (2011) has illustrated that this influx effect could impact on Mg isotope systematics and for epsomite and the study has substantially evaluated this impact. These authors found that replenishing 70% of the brine could generate relatively uniform Mg isotopic compositions in epsomite. However, the absence of lithostratigraphic evidence for an influx event, argues against influx as a mechanism for creating the Salado langbeinites. Moreover, langbeinite generally precipitates during the final stages of evaporite formation and is a highly soluble mineral phase (Warren, 2010). Thus, a massive seawater influx would likely dissolve the preexisting (underlying) and soluble phases, and hence resetting the whole evaporite system and preventing langbeinite preservation. Therefore, we see no evidence of massive seawater influx in this time interval to explain the observed Salado langbeinite's uniform δ^{26}Mg values.

In addition, recrystallization is also another candidate explanation of the Salado langbeinite's uniform δ^{26}Mg values since recrystallization may potentially reset and homogenize isotopic compositions at the mineral scale. Field observations have documented numerous examples of secondary textures within the Salado Formation (Lowenstein & Spencer, 1990). While recrystallization may have caused some of the homogeneity in the Salado langbeinite's Mg isotopic compositions, the massive scale of the deposit (~100 m) argues against recrystallization as the only mechanism for the observed signatures.

On the other hand, rapid precipitation and associated kinetic processes may also account for uniformity of the observed Mg isotopic compositions. Uniform sulfur isotopic composition observed in langbeinite samples ($10.05 \pm 0.27‰$, $10.11‰$, and $10.78 \pm 0.39‰$ for mean δ^{34}S; Renne et al., 2001) support this mechanism. Rapid growth typically occurs in cold, arid environments where sublimation can occur or in relatively warm climates (Warren, 1999, 2010). Langbeinite's relatively high precipitation temperature (Braitsch, 1964, 1971) raises the possibility that the Salado langbeinite developed in a sabkha, salt pan, or salina, which often form in warm climates with high evaporation rates. If rapid precipitation caused the uniform δ^{26}Mg values in the Salado langbeinites, the 100 m thickness of the deposit suggests fairly high ambient temperatures driving evaporation. The formation of this langbeinite sequence may have occurred in a stagnant environment that facilitated rapid evaporation. Furthermore, this inference implies that even if the Delaware Basin represents an open ocean depositional setting prior to langbeinite precipitation, the depositional environment may have transitioned to a shallow and relatively restricted setting by the Late Permian. Paleoreconstructions situating the Salado basin close to the paleo-equator support the interpretation of warm climatic conditions. Biostratigraphic evidence (Brezinski, 1992) and crystallization temperatures (average of 71°C) estimated from Salado halite fluid inclusions (Lowenstein & Spencer, 1990) also support interpretations of warm, arid conditions for the basin. The conditions implied by Mg isotopic signatures are thus consistent with the overall interpretation of the Salado Formation as a shallow, marginal basin experiencing desiccation during the latest Permian (Holser & Magaritz, 1987; Lowenstein, 1988; Renne et al., 2001).

6. Interpretation of Brine Source

Understanding brine source and evolution is critical for reconstructing the evaporation history and understanding the origin of the evaporite deposit. Researchers have debated whether brines forming the Salado evaporites represented purely marine or mixed sources, or formed during postdiagenesis (e.g., Bein et al., 2015; Knauth & Beeunas, 1986; Lowenstein, 1988; Lowenstein & Spencer, 1990). The source of the brines forming these Late Permian evaporite deposits is a central issue in age interpretations of cryptic, halotolerant bacteria (Vreeland et al., 2000), and can help inform understanding of the bacteria's origin and history.

Strontium isotopes are commonly used to track brine source in evaporites because (1) seawater, fresh water (even individual rivers), and meteoric water each have unique $^{87/86}$Sr isotopic signatures, and (2) $^{87/86}$Sr isotopic ratios are typically thought to be preserved by evaporites from parent brines without obvious Sr

isotopic variation (i.e., Kirkland et al., 2000; Denison et al., 1998; Edmond, 1992). The Sr system ideally records relative seawater and fresh water input to the parent brine as values falling along a two end member mixing line. Kirkland et al. (2000) proposed that the Upper Permian Castile Formation, which underlies the Salado Formation, came from a marine source based on matching $^{87}Sr/^{86}Sr$ values for the Castile evaporites with the inferred early Ochoan seawater. However, because evaporites inherit the $^{87/86}Sr$ isotopic features of their parent brine, the range of $^{87/86}Sr$ ratios of evaporite falls within the range composed of fresh water and marine water. Even if a brine fluid interacts with evaporites like what a diagenetic fluid does, its $^{87}Sr/^{86}Sr$ values still fall within the range composed of fresh water and marine water. Therefore, the $^{87}Sr/^{86}Sr$ ratios of the evaporite which is derived from a such brine (i.e., diagenetic fluid) would not be distinctive from the regular water range. In other words, $^{87}Sr/^{86}Sr$ value of evaporites is not a sensitive tool tracing the diagenetic brine source.

Magnesium isotopes may alternatively help elucidate diagenetic brine characteristics, since Mg isotopes show large fractionations and different fractionation directions for silicate and carbonate-solution systems (Galy et al., 2002; Higgins & Schrag, 2010; Immenhauser et al., 2010; Li et al., 2012, 2015; Mavromatis et al., 2012, 2013; Pearce et al., 2012; Pogge von Strandmann, 2008; Rustad et al., 2010; Saulnier et al., 2012; Schauble, 2011; Wang et al., 2013; Young & Galy, 2004). Here we used theoretically predicted Mg isotopic fractionation factor to estimate conditions of the initial Salado langbeinite brine. This approach modeled Mg isotopic evolution of a brine at equilibrium over the whole Mg-bearing deposit to estimate the nondiagenetic parent brine's Mg isotopic composition for langbeinite. We can then compare the estimated δ^{26}Mg composition of brine with the values measured from natural langbeinite (around $-4\,‰$).

We assumed that the Mg isotopic composition of Ochoan seawater resembled that of modern seawater (δ^{26}Mg of $-0.8‰$, Teng et al., 2015; Tipper et al., 2006b) and used Mg isotopic fractionation factors for mineral-solution systems reported in Higgins and Schrag (2010): $^{26/24}\alpha_{\text{Mg clay-water}} = 1.0007$ and $^{26/24}\alpha_{\text{dolomite-water}} = 0.9980$ at low temperatures. Lithologic observations (see Figure 1) indicate that carbonates and clay minerals were important Mg-bearing constituents in the other underlying depositional sequences (Abitz et al., 1990; Anderson 1981; Stein & Krumhansl, 1988). Calcite is typically present with poor siliclastic in the Rustler Formation, whereas calcite and magnesite are usually interbedded with clay minerals in the Salado Formation. Since carbonates and clay exhibit opposite Mg isotopic fractionation directions, δ^{26}Mg values estimated for the evolving brine would be obscured by the interbedded stratigraphy. We therefore simplified underlying strata as separate carbonate and Mg-clay layers. According to Rayleigh equation (7) $\delta_w = (\delta_0 + 1000) \cdot f^{(\alpha_{langb-water}-1)} - 1000$, we can calculate the$\delta^{26}$Mg of the brine as:

$$\delta^{26}\text{Mg}_{\text{brine}} = \left(\delta^{26}\text{Mg}_0 + 1000\right) * \text{f}^{(\alpha\text{mineral}-\text{water}-1)} - 1000.$$

where $\delta^{26}Mg_0$ is the initial δ^{26}Mg of the brine solution, f = 1-F, F is the precipitated fraction of Mg in the mineral. The volum fraction of calcite in underlying Rustler Formation is 5% (see in Figure 1). The precise fraction of carbonates and clay in our sampling McNutt unit and the underlying lower unit of Salado Formation is unclear, but both of the fraction of these two components are small (<5%) based on the field observation. If we consider the contribution of the 5% calcite of overlying Rustler Formation, we can approximately assume that the Ochoan seawater precipitated Mg fraction of 2:1 for carbonates and clay, respectively. Since most of the Mg would remain in the seawater, we assume F values of 5% and 10% for Mg-clay and carbonate, respectively (carbonates predominate). Assuming Ochoan seawater initially precipitated the carbonate layer and then formed the Mg-clay, the model estimates δ^{26}Mg values of $-0.589‰$ for the brine after carbonate precipitation. This becomes the $\delta^{26}Mg^0_{\text{brine}}$ for subsequent Mg-clay formation. The model gets an estimated δ^{26}Mg values to $-0.641‰$ for the brine after Mg-clay formation. This value evoluted from a starting seawater value is far higher than the initial value (–4‰) previously estimated for the Salado langbeinite.

We suggest that the brine source of Salado Formation is also not a result of a hybrid source mixing with fresh water. The range of δ^{26}Mg values for river and groundwater sources (Figure 5) demonstrate that isotopically light fresh water sources would still not suffice to shift brine values all the way to the observed $-4‰$. Therefore, we suggest that a brine, which is evolved from marine water or simply mixing fresh water, could not be the source of the Salado langbeinite evaporites.

Instead, we propose that Salado langbeinite brine maybe derived from the fluids which experienced intensive interactions with Mg-clay minerals to finally get a light Mg isotopic composition due to $\alpha_{\text{Mg clay-water}} > 1$.

These fluids could represent pore water produced by the Mg-clay removal during diagenesis, for example. Depleted δ^{26}Mg values have also been documented from sediment pore fluids, which showed δ^{26}Mg declining from surface values of $-0.75‰$ to $-2.56‰$ as the removal of Mg-clay increases (Higgins & Schrag, 2010). This diagenetic history could help further constrain the conditions under which langbeinite forms.

7. Conclusions

This study reports Mg isotopic values and systematics for a thick langbeinite evaporite accumulation. Results were interpreted according to the theoretical equilibrium fractionation factors calculated for langbeinite and its parent brine. These were used to reconstruct the brine evolution and depositional environment. Langbeinite from the Late Permian Salado Formation records light Mg isotopic compositions relative to modern seawater. In contrast to the δ^{26}Mg profiles published for some carbonate assemblages, δ^{26}Mg values for Salado langbeinite samples are relatively uniform. The uniformity of these values may arise from recrystallization or influx of additional seawater but geochemical or lithostratigraphic evidence for these mechanisms is lacking. Both the equilibrium and rapid kinetic formation processes require elevated temperatures in the depositional environment. Precipitation of the Salado langbeinite in a warm, arid environment is consistent with both Mg isotopic signatures and other lines of stratigraphic evidence concerning depositional environment of the Delaware Basin in the Late Permian. This study demonstrates that Mg isotopes of sulfate evaporites can be used to constrain the brine source, and other critical information on how evaporites form.

Acknowledgments
Data supporting Figure 2 are available from https://www2.nau.edu/rcb7/globaltext2.html. Data supporting Figures 3–6 are available in supporting information Data sets S1–S4. We thank Yusuke Yokoyama for his expert editorial handling and two anonymous reviewers for providing helpful comments that significantly enhanced the quality of the manuscript. We also gratefully thank Prof. Yun Liu and Prof. Fang Huang for providing constructive feedback and commentary, and M. Sanborn for reading through the manuscript and editing English. This work was supported by the Natural Science Foundation of China (41530210).

References

Abitz, R., Myers, J., Drez, P., & Deal, D. (1990). Geochemistry of Salado Formation Brines Recovered from the Waste Isolation Pilot Plant (WIPP) Repository (No. CONF-900210-63). Paper presented at the Symposium on Waste Manage, Albuquerque, New Mexico, USA. Retrieved from http://www.iaea.org/inis/collection/NCLCollectionStore/_Public/22/064/22064156.pdf

Akilan, C., Rohman, N., Hefter, G., & Buchner, R. (2006). Temperature effects on ion association and hydration in $MgSO_4$ by dielectric spectroscopy. *ChemPhysChem*, *7*(11), 2319–2330.

Anderson, R. Y. (1981). Deep-seated salt dissolution in the Delaware Basin, Texas and New Mexico. Environmental geology and hydrology in New Mexico. *New Mexico Geological Society Special Publication*, 10, 133–145.

Baker, J. A., Schiller, M., & Bizzarro, M. (2012). 26Al–26 Mg deficit dating ultramafic meteorites and silicate planetesimal differentiation in the early Solar System? *Geochimica et Cosmochimica Acta*, *77*, 415–431.

Bein, A., Hovorka, S. D., Fisher, R. S., & Roedder, E. (2015). Fluid inclusions in bedded permian halite, palo duro basin, texas: Evidence for modification of seawater in evaporite brine-pools and subsequent early diagenesis. *Journal of Sedimentary Research*, *61*(1), 1–14.

Bigeleisen, J., & Mayer, M. G. (1947). Calculation of equilibrium constants for isotopic exchange reactions. *The Journal of Chemical Physics*, *15*(5), 261–267.

Black, J. R., Epstein, E., Rains, W. D., Yin, Q-Z., & Casey, W. H. (2008). Magnesium-isotope fractionation during plant growth. *Environmental Science & Technology*, *42*(21), 7831–7836.

Blakey, R. (2004). Paleogeographic reconstructions. Arizona: University of Arizona. Retrieved from http://jan.ucc.nau.edu/~rcb7/270NAt.jpg

Blattler, C. L., Miller, N. R., & Higgins, J. A. (2015). Mg and Ca isotope signatures of authigenic dolomite in siliceous deepsea sediments. *Earth and Planetary Science Letters*, *419*, 32–42.

Braitsch, O. (1964). *The temperature of evaporite formation*. In A. E. M. Nairn (Ed.), *Problems in palaeoclimatology* (pp. 479–490). Geneva, Switzerland: Inderscience Publishers.

Braitsch, O. (1971). *Salt deposits their origin and composition* (Vol. 4). Berlin, Germany: Springer Science & Business Media. Retrieved from https://link.springer.com/book/10.1007/978-3-642-65083-3

Brezinski, D. K. (1992). Permian trilobites from west Texas. *Journal of Paleontology*, *66*(6), 924–943.

Buchner, R., Chen, T., & Hefter, G. (2004). Complexity in "simple" electrolyte solutions: Ion pairing in $MgSO_{4(aq)}$. *Journal of Physical Chemistry B*, *108*(7), 2365–2375.

Buhl, D., Immenhauser, A., Smeulders, G., Kabiri, L., & Richter, D. K. (2007). Time series d26Mg analysis in speleothem calcite: Kinetic versus equilibrium fractionation, comparison with other proxies and implications for palaeoclimate research. *Chemical Geology*, *244*(3–4), 715–729.

Chang, V. T.-C., Makishima, A., Belshaw, N. S., & O'Nions, R. K. (2003). Purification of Mg from low-Mg biogenic carbonates for isotope ratio determination using multiple collector ICP-MS. *Journal of Analytical Atomic Spectrometry*, *18*(4), 296–301.

Denison, R. E., Kirkland, D. W., & Evans, R. (1998). Using strontium isotopes to determine the age and origin of gypsum and anhydrite beds. *The Journal of Geology*, *106*(1), 1–18.

Dessert, C., Lajeunesse, E., Lloret, E., Clergue, C., Crispi, O., Gorge, C., & Quidelleur, X. (2015). Controls on chemical weathering on a mountainous volcanic tropical island: Guadeloupe (French West Indies). *Geochimica et Cosmochimica Acta*, *171*, 216–237.

DePaolo, D. J. (2011). Surface kinetic model for isotopic and trace element fractionation during precipitation of calcite from aqueous solutions. *Geochimica et Cosmochimica Acta*, *75*(4), 1039–1056.

Edmond, J. M. (1992). Himalayan tectonics, weathering processes, and the strontium isotope record in marine limestones. *Science*, *258*(5088), 1594–1597.

Fantle, M. S., & Higgins, J. (2014). The effects of diagenesis and dolomitization on Ca and Mg isotopes in marine platform carbonates: Implications for the geochemical cycles of Ca and Mg. *Geochimica et Cosmochimica Acta*, *142*, 458–481.

Feng, C., Qin, T., Huang, S., Wu, Z., & Huang, F. (2014). First-principles investigations of equilibrium calcium isotope fractionation between clinopyroxene and Ca-doped orthopyroxene. *Geochimica et Cosmochimica Acta*, *143*, 132–142.

Forney, G. G. (1975). Permo-Triassic sea-level change. *The Journal of Geology*, *83*(6), 773–779.
Frisch, M., Trucks, G., Schlegel, H., Scuseria, G., Robb, M., Cheeseman, J., et al. (2009). *Gaussian 09, revision A. 1*. Wallingford, CT: Gaussian, Inc.
Galy, A., Bar-Matthews, M., Halicz, L., & O'nions, R. K. (2002). Mg isotopic composition of carbonate: Insight from speleothem formation. *Earth and Planetary Science Letters*, *201*(1), 105–115.
Galy, A., Yoffe, O., Janney, P. E., Williams, R. W., Cloquet, C., Alard, O., et al. (2003). Magnesium isotope heterogeneity of the isotopic standard SRM980 and new reference materials for magnesium-isotope-ratio measurements. *Journal of Analytical Atomic Spectrometry*, *18*(11), 1352–1356.
Golonka, J., Ross, M., & Scotese, C. (1994). Phanerozoic paleogeographic and paleoclimatic modeling maps. In A. F. Ambry, B. Beauchamp, & D. J. Glass (Eds.), *Pangaea: Global environment and resources. Canadian Society of Petroleum Geologists, Memoir* (Vol. 17, pp. 1–47). Calgary, Canada: Canadian Society of Petroleum Geologists.
He, H. T., Zhang, S. T., Zhu, C., & Liu, Y. (2016). Equilibrium and kinetic Si isotope fractionation factors and their implications for Si isotope distributions in the Earth's surface environments. *Acta Geochimica*, *35*(1), 15–24.
Higgins, J. A., & Schrag, D. P. (2010). Constraining magnesium cycling in marine sedi-ments using magnesium isotopes. *Geochimica et Cosmochimica Acta*, *74*(17), 5039–5053.
Higgins, J. A., & Schrag, D. P. (2012). Records of Neogene seawater chemistry and diagenesis in deep-sea carbonate sediments and pore fluids. *Earth and Planetary Science Letters*, *357–358*, 386–396.
Higgins, J. A., & Schrag, D. P. (2015). The Mg isotopic composition of Cenozoic seawater—evidence for a link between Mg-clays, seawater Mg/Ca, and climate. *Earth and Planetary Science Letters*, *416*, 73–81.
Holser, W., & Magaritz, M. (1987). Events near the Permian-Triassic boundary. *Modern Geology*, *11*, 155–180.
Hu, Y., Teng, F. Z., Plank, T., & Huang, K. J. (2017). Magnesium isotopic composition of subducting marine sediments. *Chemical Geology*, *466*, 15–31.
Huang, F., Chen, L., Wu, Z., & Wang, W. (2013). First-principles calculations of equilibrium Mg isotope fractionations between garnet, clinopyroxene, orthopyroxene, and olivine: implications for Mg isotope thermometry. *Earth and Planetary Science Letters*, *367*, 61–70.
Immenhauser, A., Buhl, D., Richter, D., Niedermayr, A., Riechelmann, D., Dietzel, M., et al. (2010). Magnesium isotope fractionation during low-Mg calcite precipitation in a limestone cave- Field study and experiments. *Geochimica et Cosmochimica Acta*, *74*(15), 4346–4364.
Jacobson, A. D., Zhang, Z., Lundstrom, C., & Huang, F. (2010). Behavior of Mg isotopes during dedolomitization in the Madison Aquifer, South Dakota. *Earth and Planetary Science Letters*, *297*(3–4), 446–452.
Jacobsen, B., Yin, Q-Z., Moynier, F., Amelin, Y., Krot, A. N., Nagashima, K., et al. (2008). 26 Al–26 Mg and 207 Pb–206 Pb systematics of Allende CAIs: Canonical solar initial 26 Al/27 Al ratio reinstated. *Earth and Planetary Science Letters*, *272*(1–2), 353–364.
Jahn, S., & Schmidt, C. (2010). Speciation in aqueous $MgSO_4$ fluids at high pressures and high temperatures from ab initio molecular dynamics and Raman spectroscopy. *Journal of Physical Chemistry B*, *114*(47), 15565–15572.
Javoy, M., Balan, E., Méheut, M., Blanchard, M., & Lazzeri, M. (2012). First-principles investigation of equilibrium isotopic fractionation of O- and Si-isotopes between refractory solids and gases in the solar nebula. *Earth and Planetary Science Letters*, *319–320*, 118–127.
Kapitán, J., Dracínský, M., Kaminský, J., Benda, L., & Bour, P. (2010). Theoretical modeling of magnesium ion imprints in the Raman scattering of water. *The Journal of Physical Chemistry B*, *114*(10), 3574–3582.
Kasemann, S. A., Pogge von Strandmann, P. A. E., Prave, A. R., Fallick, A. E., Elliott, T., & Hoffmann, K. H. (2014). Continental weathering following a Cryogenian glaciation: Evidence from calcium and magnesium isotopes. *Earth and Planetary Science Letters*, *396*, 66–77.
Kirkland, D. W., Denison, R. E., & Dean, W. E. (2000). Parent brine of the castile evaporites (Upper Permian), Texas and New Mexico. *Journal of Sedimentary Research*, *70*(3), 749.
Knauth, L. P., & Beeunas, M. A. (1986). Isotope geochemistry of fluid inclusions in permian halite with implications for the isotopic history of ocean water and the origin of saline formation waters. *Geochimica et Cosmochimica Acta*, *50*(3), 419–433.
Kowalski, P. M., Wunder, B., & Jahn, S. (2013). Ab initio prediction of equilibrium boron isotope fractionation between minerals and aqueous fluids at high P and T. *Geochimica et Cosmochimica Acta*, *101*, 285–301.
Kutzbach, J., & Gallimore, R. (1989). Pangaean climates: Megamonsoons of the megacontinent. *Journal of Geophysical Research*, *94*(D3), 3341–3357.
Lee, S. W., Ryu, J. S., & Lee, K. S. (2014). Magnesium isotope geochemistry in the Han River, South Korea. *Chemical Geology*, *364*, 9–19.
Li, W., Beard, B. L., & Johnson, C. M. (2011). Exchange and fractionation of Mg isotopes between epsomite and saturated $MgSO_4$ solution. *Geochimica et Cosmochimica Acta*, *75*(7), 1814–1828.
Li, W., Beard, B. L., Li, C., Xu, H., & Johnson, C. M. (2015). Experimental calibration of Mg isotope fractionation between dolomite and aqueous solution and its geological implications. *Geochimica et Cosmochimica Acta*, *157*, 164–181.
Li, W., Chakraborty, S., Beard, B. L., Romanek, C. S., & Johnson, C. M. (2012). Magnesium isotope fractionation during precipitation of inorganic calcite under laboratory conditions. *Earth and Planetary Science Letters*, *333–334*, 304–316.
Li, X., Zhao, H., Tang, M., & Liu, Y. (2009). Theoretical prediction for several important equilibrium Ge isotope fractionation factors and geological implications. *Earth and Planetary Science Letters*, *287*(1–2), 1–11.
Li, X. F., & Liu, Y. (2010). First-principles study of Ge isotope fractionation during adsorption onto Fe (III)-oxyhydroxide surfaces. *Chemical Geology*, *278*(1–2), 15–22.
Li, X. F., & Liu, Y. (2015). A theoretical model of isotopic fractionation by thermal diffusion and its implementation on silicate melts. *Geochimica et Cosmochimica Acta*, *154*, 18–27.
Liu, C., Wang, Z., Raub, T. D., Macdonald, F. A., & Evans, D. A. D. (2014). Neoproterozoic cap-dolostone deposition in stratified glacial meltwater plume. *Earth and Planetary Science Letters*, *404*, 22–32.
Liu, Y., & Tossell, J. A. (2005). Ab initio molecular orbital calculations for boron isotope fractionations on boric acids and borates. *Geochimica et Cosmochimica Acta*, *69*(16), 3995–4006.
Liu, Y. (2013). *On the test of a new volume variable cluster model method for stable isotopic fractionation of solids: Equilibrium Mg isotopic fractionations between minerals and solutions*. Abstract presented at 2013 Goldschmidt Conference (Vol. 1632). Florence, Italy: Geochemical Society & European Association of Geochemistry.
Lowenstein, T. K. (1988). Origin of depositional cycles in a Permian "saline giant": The Salado (McNutt zone) evaporites of New Mexico and Texas. *Geological Society of America Bulletin*, *100*(4), 592–608.
Lowenstein, T. K., & Spencer, R. J. (1990). Syndepositional origin of potash evaporites; petrographic and fluid inclusion evidence. *American Journal of Science*, *290*(1), 1–42.
Ma, L., Teng, F. Z., Jin, L., Ke, S., Yang, W., Gu, H. O., et al. (2015). Magnesium isotope fractionation during shale weathering in the Shale Hills Critical Zone Observatory: Accumulation of light Mg isotopes in soils by clay mineral transformation. *Chemical Geology*, *397*, 37–50.

Markham, G. D., Glusker, J. P., & Bock, C. W. (2002). The arrangement of first-and second-sphere water molecules in divalent magnesium complexes: Results from molecular orbital and density functional theory and from structural crystallography. *The Journal of Physical Chemistry B*, *106*(19), 5118–5134.

Mavromatis, V., Gautier, Q., Bosc, O., & Schott, J. (2013). Kinetics of Mg partition and Mg stable isotope fractionation during its incorporation in calcite. *Geochimica et Cosmochimica Acta*, *114*, 188–203.

Mavromatis, V., Pearce, C. R., Shirokova, L. S., Bundeleva, I. A., Pokrovsky, O. S., Benezeth, P., et al. (2012). Magnesium isotope fractionation during hydrous magnesium carbonate precipitation with and without cyanobacteria. *Geochimica et Cosmochimica Acta*, *76*, 161–174.

Méheut, M., Lazzeri, M., Balan, E., & Mauri, F. (2007). Equilibrium isotopic fractionation in the kaolinite, quartz, water system: Prediction from first-principles density-functional theory. *Geochimica et Cosmochimica Acta*, *71*(13), 3170–3181.

Mereiter, K. (1979). Refinement of the crystal structure of langbeinite $K_2Mg_2(SO_4)_3$. *Neues Jahrbuch Für Mineralogie, Monatshefte* (pp. 182–188). Stuttgart, Germany: Neues Jahrbuch für Geologie und Paläontologie.

Millero, F. J. (1974). The physical chemistry of seawater. *Annual Review of Earth and Planetary Sciences*, *2*(1), 101–150.

Mink, J., Németh, C., Hajba, L., Sandström, M., & Goggin, P. (2003). Infrared and Raman spectroscopic and theoretical studies of hexaaqua metal ions in aqueous solution. *Journal of Molecular Structure*, *661–662*, 141–151.

Ohtaki, H., & Radnai, T. (1993). Structure and dynamics of hydrated ions. *ChemInform*, *24*(31), 1157–1204.

Opfergelt, S., Burton, K. W., Georg, R. B., West, A. J., Guicharnaud, R. A., Sigfusson, B., et al. (2014). Magnesium retention on the soil exchange complex controlling Mg isotope variations in soils, soil solutions and vegetation in volcanic soils, Iceland. *Geochimica et Cosmochimica Acta*, *125*, 110–130.

Parrish, J. M., Parrish, J. T., & Ziegler, A. M. (1986). Permian-Triassic paleogeography and paleoclimatology and implications for therapsid distribution. In Hotton, N. III et al. (Eds.), *The ecology and biology of mammal-like reptiles* (pp. 109–132). Washington, DC: Smithsonian Press.

Pearce, C. R., Saldi, G. D., Schott, J., & Oelkers, E. H. (2012). Isotopic fractionation during congruent dissolution, precipitation and at equilibrium: Evidence from Mg isotopes. *Geochimica et Cosmochimica Acta*, *92*, 170–183.

Pinilla, C., Blanchard, M., Balan, E., Natarajan, S. K., Vuilleumier, R., & Mauri, F. (2015). Equilibrium magnesium isotope fractionation between aqueous Mg^{2+} and carbonate minerals: Insights from path integral molecular dynamics. *Geochimica et Cosmochimica Acta*, *163*, 126–139.

Pogge von Strandmann, P. A. (2008). Precise magnesium isotope measurements in core top planktic and benthic foraminifera. *Geochemistry, Geophysics, Geosystems*, *9*, Q12015. https://doi.org/10.1029/2008GC002209

Pogge von Strandmann, P. A., Opfergelt, S., Lai, Y. J., Sigfusson, B., Gislason, S. R., & Burton, K. W. (2012). Lithium, magnesium and silicon isotope behaviour accompanying weathering in a basaltic soil and pore water profile in Iceland. *Earth and Planetary Science Letters*, *339–340*, 11–23.

Renne, P. R., Balco, G., Ludwig, K. R., Mundil, R., & Min, K. (2011). Response to the comment by W.H. Schwarz et al. on "Joint determination of ^{40}K decay constants and $^{40}Ar^*/^{40}K$ for the Fish Canyon sanidine standard, and improved accuracy for $^{40}Ar/^{39}Ar$ geochronology" by P.R. Renne et al. (2010). *Geochimica et Cosmochimica Acta*, *75*, 5097–5100.

Renne, P. R., Sharp, W. D., Montañez, I. P., Becker, T. A., & Zierenberg, R. A. (2001). $^{40}Ar/^{39}Ar$ dating of Late Permian evaporites, southeastern New Mexico, USA. *Earth and Planetary Science Letters*, *193*(3–4), 539–547.

Rustad, J. R., & Bylaska, E. J. (2007). Ab initio calculation of isotopic fractionation in $B(OH)_3$ (aq) and BOH_4^-(aq). *Journal of the American Chemical Society*, *129*(8), 2222–2223.

Rustad, J. R., Casey, W. H., Yin, Q.-Z., Bylaska, E. J., Felmy, A. R., Bogatko, S. A., et al. (2010). Isotopic fractionation of Mg^{2+}(aq), Ca^{2+}(aq), and Fe^{2+}(aq) with carbonate minerals. *Geochimica et Cosmochimica Acta*, *74*(22), 6301–6323.

Saulnier, S., Rollion-Bard, C., Vigier, N., & Chaussidon, M. (2012). Mg isotope fractionation during calcite precipitation: An experimental study. *Geochimica et Cosmochimica Acta*, *91*, 75–91.

Schauble, E. A. (2011). First-principles estimates of equilibrium magnesium isotope fractionation in silicate, oxide, carbonate and hexaaquamagnesium (2+) crystals. *Geochimica Et Cosmochimica Acta*, *75*(3), 844–869.

Scotese, C. (1994). Late Permian paleogeographic map. Pangea: Paleoclimate, Tectonics, and Sedimentation during Accretion, Zenith and Breakup of a Supercontinent. *Special Paper Geological Society of America*, *288*, 232–242.

Shalev, N., Lazar, B., Halicz, L., & Ittai, G. (2014). *Magnesium isotopic fractionation between Mg salts and brine in the course of evaporation of marine derived brines*. Abstract presented at the 2014 EGU, Vienna, Austria.

Speer, D., & Salje, E. (1986). Phase transitions in langbeinites I: Crystal chemistry and structures of K-double sulfates of the langbeinite type $M_2^{++}K_2(SO_4)_3$, M^{++}= Mg, Ni, Co, Zn, Ca. *Physics and Chemistry of Minerals*, *13*(1), 17–24.

Stein, C., & Krumhansl, J. (1988). A model for the evolution of brines in salt from the lower Salado Formation, southeastern New Mexico. *Geochimica et Cosmochimica Acta*, *52*(5), 1037–1046.

Teng, F.-Z., Li, W.-Y., Ke, S., Yang, W., Liu, S.-A., Sedaghatpour, F., . . . et al. (2015). Magnesium isotopic compositions of international geological reference materials. *Geostandards and Geoanalytical Research*, *39*(3), 329–339.

Tipper, E. T., Calmels, D., Gaillardet, J., Louvat, P., Capmas, F., & Dubacq, B. (2012). Positive correlation between Li and Mg isotope ratios in the river waters of the Mackenzie Basin challenges the interpretation of apparent isotopic fractionation during weathering. *Earth and Planetary Science Letters*, *333–334*, 35–45.

Tipper, E., Galy, A., & Bickle, M. J. (2006). Riverine evidence for a fractionated reservoir of Ca and Mg on the continents: Implications for the oceanic Ca cycle. *Earth and Planetary Science Letters*, *247*(3–4), 267–279.

Tipper, E. T., Galy, A., & Bickle, M. J. (2008). Calcium and magnesium isotope systematics in rivers draining the Himalaya–Tibetan-Plateau region: Lithological or fractionation control?. *Geochimica et Cosmochimica Acta*, *72*(4), 1057–1075.

Tipper, E. T., Galy, A., Gaillardet, J., Bickle, M., Elderfield, H., & Carder, E. (2006). The magnesium isotope budget of the modern ocean: Constraints from riverine magnesium isotope ratios. *Earth and Planetary Science Letters*, *250*(1–2), 241–253.

Tipper, E. T., Lemarchand, E., Hindshaw, R. S., Reynolds, B. C., & Bourdon, B. (2012). Seasonal sensitivity of weathering processes: Hints from magnesium isotopes in a glacial stream. *Chemical Geology*, *312–313*, 80–92.

Urey, H. C. (1947). The thermodynamic properties of isotopic substances. *Journal of the Chemical Society (Resumed)*, 562–581.

Vreeland, R. H., Rosenzweig, W. D., & Powers, D. W. (2000). Isolation of a 250 million-year-old halotolerant bacterium from a primary salt crystal. *Nature*, *407*(6806), 897–900.

Wang, Z., Hu, P., Gaetani, G., Liu, C., Saenger, C., Cohen, A., et al. (2013). Experimental calibration of Mg isotope fractionation between aragonite and seawater. *Geochimica et Cosmochimica Acta*, *102*, 113–123.

Warren, J. (1999). *Evaporites: Their evolution and economics*. Hoboken, NJ: Blackwell Science Inc.

Warren, J. K. (2010). Evaporites through time: Tectonic, climatic and eustatic controls in marine and nonmarine deposits. *Earth-Science Reviews*, *98*(3–4), 217–268.

Wimpenny, J., Colla, C. A., Yin, Q. Z., Rustad, J. R., & Casey, W. H. (2014). Investigating the behaviour of Mg isotopes during the formation of clay minerals. *Geochimica et Cosmochimica Acta*, *128*, 178–194.

Wombacher, F., Eisenhauer, A., Böhm, F., Gussone, N., Regenberg, M., Dullo, W.-C., et al. (2011). Magnesium stable isotope fractionation in marine biogenic calcite and aragonite. *Geochimica et Cosmochimica Acta*, *75*(19), 5797–5818.

Wright, J., & Colling, A. and Open University. Oceanography Course Team (1995). *Seawater: Its composition, properties, and behaviour* (2nd ed./rev. for the course team by John Wright and Angela Colling). Oxford, UK: Pergamon Press, in association with the Open University, Oxford [England]; New York.

Wu, F., Qin, T., Li, X., Liu, Y., Huang, J. H., Wu, Z., et al. (2015). First-principles investigation of vanadium isotope fractionation in solution and during adsorption. *Earth & Planetary Science Letters*, *426*, 216–224.

Young, E. D., & Galy, A. (2004). The isotope geochemistry and cosmochemistry of magnesium. *Geochemistry of Non-Traditional Stable Isotopes*, *55*(1), 197–230.

Young, E. D., Manning, C. E., Schauble, E. A., Shahar, A., Macris, C. A., Lazar, C., et al. (2015). High-temperature equilibrium isotope fractionation of non-traditional stable isotopes: Experiments, theory, and applications. *Chemical Geology*, *395*, 176–195.